ELSEVIER
Materials Science and Engineering B73 (2000) 178–183
MATERIALS SCIENCE & ENGINEERING B
www.elsevier.com/locate/mseb

Wet-chemical passivation of Si(111)- and Si(100)-substrates

H. Angermann [a,*], W. Henrion [a], A. Röseler [b], M. Rebien [a]

[a] *Hahn-Meitner-Institut, Abteilung Photovoltaik Rudower Chaussee 5, D-12489 Berlin, Germany*
[b] *Institut für Spektrochemie und angewandte Spektroskopie, Rudower Chaussee 5, D-12489 Berlin, Germany*

Abstract

The influence of preparation-induced surface roughness, as well as the hydrogen and oxide coverage on electronic properties of Si(111) and Si(100) surfaces was investigated by combining various surface-sensitive techniques. Simultaneous surface photovoltage (SPV) and spectroscopic ellipsometry (SE) measurements, both in the ultraviolet/visible (UV–VIS) and the infrared (IR) spectroscopic region, yielded detailed information about intrinsic and extrinsic surface states on hydrogen (H)-terminated Si(111) and Si(100) surfaces, immediately after the wet-chemical preparation as well as during the initial oxidation. The energetic distributions of interface states $D_{it}(E)$ on Si(100) and Si(111) surfaces were correlated to the surface roughness $\langle d_r \rangle$, the change of hydrogen coverage and the oxide growth on an atomic scale. As shown by these experiments, generally higher interface state densities $D_{it,\,min}$ were observed on Si(100) surfaces in comparison to Si(111). However, on Si(100) substrates a faster oxide growth and a significantly thicker final native oxide layer were found. The wet-chemical preparation methods of hydrogen or oxide passivated surfaces on Si(100) substrates were carefully optimized, resulting in smooth H-terminated surfaces ($\langle d_r \rangle \approx 4$ Å and $D_{it,\,min} < 5 \times 10^{10}$ cm^{-2} eV^{-1}) and passivating oxide layers in the thickness range of 1–3 nm ($D_{it,\,min} < 5 \times 10^{11}$ eV^{-1} cm^{-2}).
© 2000 Elsevier Science S.A. All rights reserved.

Keywords: Silicon surface; H-termination; Native oxide; Surface photovoltage; Spectroscopic ellipsometry

1. Introduction

In order to remove particles, organic, and metallic contaminants, cleaning steps are applied repeatedly within the semiconductor process flow and occupy 30–40% of all the process steps [1]. Monitoring and control of surface properties during pre-cleaning treatments have recently received increasing attention. This is because the miniaturization of circuit patterns and the increasing level of density, integration, and performance require microscopically smooth, chemically and electronically passivated surfaces. The electronic interface properties of very thin oxide, epitaxial, and passivation layers are strongly influenced by the chemical integrity and morphological structure of the substrate surface prior to preparation. Therefore, controlling the flatness as well as the growth rate of native oxides on cleaned wafer surfaces is of great importance for the semiconductor process.

By application of various spectroscopic and structural methods (FT-IR, XPS, HREELS, TSD and STM [2–6]), the morphology and the chemical structure of wet-chemically treated silicon substrates has been intensively investigated in the recent years. These measurements, however, are not sensitive enough to detect the small number (typically 10^{10}–10^{14} eV^{-1} cm^{-2}) of silicon dangling bond defects which influence the electronic interface properties. As shown by our recently reported results, the combination of surface photovoltage (SPV) and spectroscopic ellipsometry (SE) measurements can serve as a very sensitive tool to investigate the correlation between surface morphology and dangling bond defects on Si(111) surfaces and Si/SiO_2 interfaces [7,8]. In this paper. we report on investigations of the micro-roughness, the hydrogen and oxide coverage, and the resulting density and energetic distribution of surface states of wet-chemically cleaned Si(100) substrates and Si(111) substrates.

* Corresponding author. Tel.: +49-30-67053-368; fax: +49-30-67053-333.
E-mail address: angermann@hmi.de (H. Angermann)

0921-5107/00/$ - see front matter © 2000 Elsevier Science S.A. All rights reserved.
PII: S0921-5107(99)00457-2

2. Preparation

The first step of the preparation procedure was a conventional RCA cleaning [9]. After removal of the native oxide in NH_4F solution, the wafers were chemically re-oxidized by four different procedures:
1. boiling solution of H_2SO_4:H_2O_2 (1:1) for 10 min — a standard procedure described by Chabal [2],
2. RCA I solution at 80°C for 10 min,
3. RCA II solution at 80°C for 10 min and
4. deionized water at 80°C for 120 min.

Finally, the hydrogen-termination was completed by placing the wafers into pure NH_4F solution (40%, pH = 7.8) for 6.5 min. To investigate the influence of the RCA cleaning process itself, smooth H-terminated samples were again treated by the conventional SC1 and SC2 processes [9]. H-terminated samples were additionally treated (180 s) in HF (48%) solution to obtain a sample with a well defined surface roughness. To improve the chemical stability of the wet-chemically treated surfaces the samples have been stored in clean-room air (temperature 25°C, humidity about 50%) and in deionized water (18 MΩ cm^{-1} resistivity at 80°C).

3. Measurements

Information on electronic interface properties was obtained from the large-signal SPY measurements. We utilized the SPV technique for the contactless measurement of the surface band-bending (Y) and the energetic distribution of surface states $D_{it}(E)$. A mica foil dielectric spacer was used in the same experimental configuration as described in [10].

A pulsed laser diode (150 ns, wavelength $\lambda = 904$ nm and power $P = 150$ W) was used to flash the sample. From the large-signal photovoltage pulse the surface potential was obtained as a function of the applied bias. $D_{it}(E)$ was calculated from the band-bending bias relationship [11].

Surface roughness $\langle d_r \rangle$ and oxide thickness $\langle d_{ox} \rangle$ on wet-chemically treated wafers were determined by UV–VIS SE. For the measurements in the photon energy range 3.2–4.5 eV at an angle of incidence of $77.00 \pm 0.02°$ a commercial Woollam VASE spectroscopic ellipsometer was used. The directly-measured complex ratio of reflection coefficients was transformed to the complex effective dielectric function $\langle \varepsilon \rangle$. Assuming appropriate models described below, values for the surface roughness and the thickness of the native oxide were calculated.

In addition, the hydrogen coverage of Si(100) and Si(111) surfaces was directly measured by sensing the Si–H and $Si(–H)_2$ vibrational resonance by Fourier-Transform infrared ellipsometry (FT-IR SE). In contrast to the attenuated total reflection (ATR) work described by Higashi et al. [12], the FT-IR SE utilizes only a single light reflection for sensing the Si–H vibrational resonance and can therefore be used for standard wafer characterization. For FT-IR SE measurements in the region of 2000–2150 cm^{-1}, a photometric ellipsometer was employed [13], which is coupled to a Fourier-Transform-Spectrometer (Bruker IFS55) set to a resolution of 4 cm^{-1}. The angle of incidence was 65° and the MCT-detector output was corrected for the non-linearity. From four polarizer settings, the $|\rho| = \tan \Psi$ and $\arg(\rho) = \Delta$ spectra were calculated. For a precise measurement of Δ in the range of $0° \leq \Delta \leq 360°$ and to reduce depolarization effects due to reflections from the sample backside, a reflection retarder (KR55-Prism) with approximately 90° retardation described by Röseler [14] was used.

4. Results

Wet-chemical cleaning methods can be classified into two groups:
1. hydrophilic methods resulting in thin native oxide layers, and
2. hydrophobic methods dissolving the native oxide completely in HF or ammoniumfluoride (NH_4F)-containing solutions [2,15]

Hydrophilic methods such as the RCA standard cleaning process [9] are mainly based on H_2O_2-containing solutions which increase the micro-roughness of the silicon interface as a side effect to the H_2O_2 decomposition. If the native oxide growth is irregular, the micro-roughness also increases after the native oxide removal.

4.1. Micro-roughness and surface state distribution of hydrophobic Si(111) and Si(100) surfaces

Although there is no clear definition of 'micro-roughness' itself, we will use the term to denote atomic scale irregularities on the silicon surface or the Si/SiO_x-interface. In the UV–VIS the optical effect of a microscopically rough surface can be described accurately [16] by a Bruggeman effective medium [17] (EMA) layer. For microscopically rough wafers we used a two-layer model that consists of bulk c-Si and a Bruggeman EMA layer consisting of 50% bulk c-Si and 50% voids.

Fig. 1a shows the imaginary part of the effective dielectric function $\langle \varepsilon_2 \rangle$ obtained by UV–VIS SE measurements immediately after a special preparation of H-terminated Si(111) and Si(100) surfaces. Whereas the surface is usually oxidized in H_2SO_4/H_2O_2 [2], for these investigations we applied a wet-chemical oxidation procedure in deionized water of 80° prior to the final etching step in NH_4F solution [7] in order to minimize the interface roughness between the substrate and the oxide layer.

The magnitude of $\langle \varepsilon_2 \rangle$ at the E_2 silicon bulk critical point energy of ≈ 4.24 eV can be taken here as a measure of the smoothness of the surface. We assume that largest $\langle \varepsilon_2 \rangle (E_2)$ means $\langle d_r \rangle = 0$. In our measurements the largest $\langle \varepsilon_2 \rangle (E_2)$ values of 47.2 (curve 1 in Fig. 1) were detected on the H-terminated Si(111) samples. The difference to the largest value given for Si [18] corresponds to a surface roughness $\langle d_r \rangle$ of about 1 Å. On H-terminated Si(100), generally higher values $\langle d_r \rangle$ of about 4 Å were found (curve 2 in Fig. 1a) which result from the anisotropic etching behavior of the NH_4F solution. On H-terminated samples additionally treated in HF solution (180 s), a higher increase in surface roughness was observed on Si(111) (curve 4 in Fig. 1a) than on Si(100).(curve 3 in Fig. 1a).

Fig. 1b shows the surface state distributions $D_{it}(E)$ obtained on the same Si(111) and Si(100) samples. The continuous energetic distribution of rechargeable interface states as determined by the SPV method can be separated into several groups of states originating from dangling bond defects with different back-bond configurations. Following the dangling bond model for the Si/SiO_2 interface [19], on the H-terminated surface two groups of intrinsic states resulting from strained ($Si_3 \equiv Si–Si \equiv Si_3$) bonds and from dangling bond defect centers back-bonded only to silicon ($Si_3 \equiv Si–$) give rise to a U-shaped distribution. The saturation of dangling bonds by hydrogen eliminates such surface states. Therefore, successfully H-terminated surfaces are characterized by such a U-shaped surface state distribution and very low minimal values ($D_{it,\ min}$) of the surface state density that result from the remaining intrinsic defects only. On the interfaces between silicon and native oxides a superposition of different contributions can be observed:

1. intrinsic states and
2. extrinsic states (P_L and P_H), which result from silicon dangling bonds on oxidized silicon atoms Si^{+1} ($Si_2O \equiv Si–$) and Si^{+2} ($SiO_2 \equiv Si–$).

Therefore, the interface state distribution is directly related to the state of oxidation of the silicon surface.

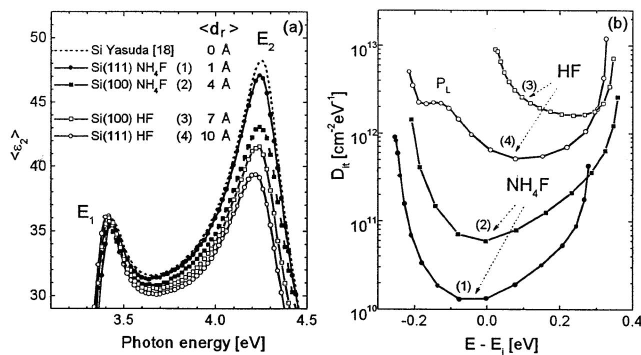

Fig. 1. Imaginary part of the effective dielectric function $\langle \varepsilon_2 \rangle$ (a) and surface state distribution $D_{it}(E)$ (b) for H-terminated NH_4F- and HF-treated Si(111) and Si(100) surfaces.

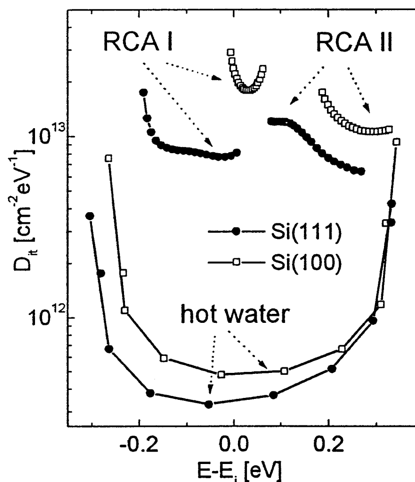

Fig. 2. Interface state distribution $D_{it}(E)$ for Si(111) and Si(100) after RCA and hot water treatment (80°C, 120 min).

As shown in Fig. 1b the lowest value of $D_{it,\ min} < 1.5 \times 10^{10}$ cm^{-2} eV^{-1} was obtained on the smoothest, H-terminated Si(111) surface (curve 1). On Si(100) surfaces typically higher values of $D_{it,\ min} < 5 \times 10^{10}$ cm^{-2} eV^{-1} were observed on wafers prepared by the floating zone technique (curve 2 in Fig. 1b) and of about 3×10^{11} cm^{-2} eV^{-1} on wafers prepared by the Czochralski technique (not shown here). A further increase of surface roughness by the HF-treatment resulted in higher surface state densities (curve 3 and 4 in Fig. 1b). Moreover, the energetic distribution of surface states changed as soon as the surface roughness exceeded two monolayers. A group of extrinsic states (PL) forming Gaussian distributions in the lower half of the forbidden gap additionally appeared. These extrinsic states have been assigned to dangling bond defects ($Si_2O \equiv Si–$) correlated to Si atoms of low state of oxidation, Si^{+1}. The occurrence of these oxygen back-bonded defects, resulting from competing reactions of various nucleophilic components (H_2O and OH^-) of the HF solution, indicated that the atomically rough HF-treated surface is not completely saturated by hydrogen.

4.2. Oxide thickness and surface state density on hydrophilic Si(111) and Si(100) surfaces

Fig. 2 presents the experimental interface state distributions $D_{it}(E)$ as typically obtained by SPV measurements of initially H-terminated Si(111) and Si(100) samples after the standard RCA I and RCA II process [9] as well as after the newly-developed hot water treatment (120 min) [8].

All conventional RCA treatments result in high densities of the extrinsic interface states corresponding to; $D_{it,\ min} > 5*10^{12}$ cm^{-2} eV^{-1} caused by the rapid and

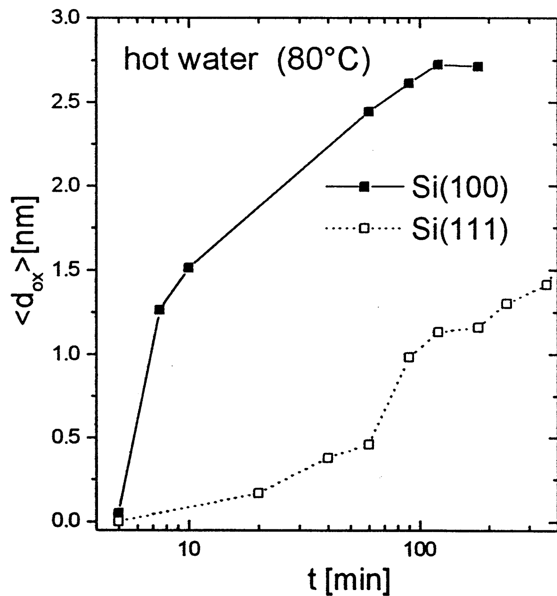

Fig. 3. Oxide thickness $\langle d_{ox}\rangle$ on previously H-terminated Si(111) and Si(100) versus the treatment time in H_2O.

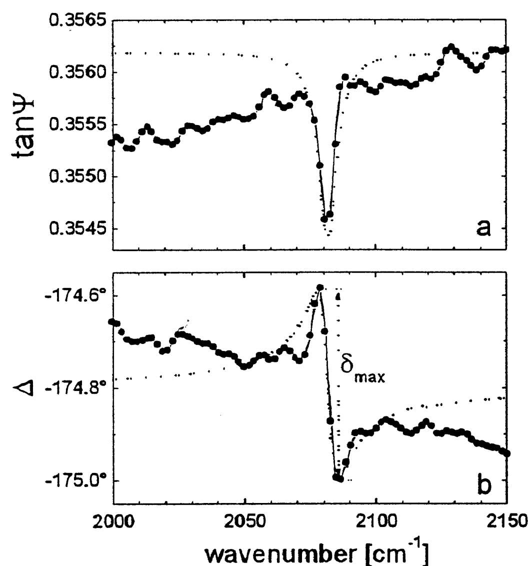

Fig. 4. Typical tan Ψ (a) and Δ (b) spectra of the Si–H bonds obtained on the H-terminated Si(111) surface.

irregular wet-chemical oxide growth. Furthermore, on RCA I treated surfaces we observed a negative charge, whereas the RCA II process, as known from CV-measurements of thermally prepared oxides, causes a positive fixed oxide charge. To avoid both irregular native oxide growth and contamination from H_2O_2-containing solutions, we started the preparation of thin passivating oxide layers on very smooth H-terminated surfaces by applying the pure water treatment at 80°C. The initial phase of this oxidation process was also characterized by a drastic increase of the density of states and the appearance of groups of extrinsic states. During the further oxidation, however, a significant decrease of the density of states as well as of the surface charge was observed which was correlated to the layer by layer formation of the Si/SiO_2 interface [8]. The final interface state density $D_{it,\,min} > 5\times10^{11}$ eV cm^{-2} (Fig. 2) of the resulting thin oxide layer on Si(111) and Si(100) surfaces was found to be lower than that of conventionally prepared chemical and thermal oxides in the thickness range of 1–3 nm. We assume that the very slow layer-by-layer oxide growth on the atomically flat H-terminated surface is due to a well-ordered interface already during the formation of the first monolayers.

4.3. Surface electronic properties during native oxide growth in water and air

Simultaneous SPV, FT-IRSE, and UV-VIS SE measurements were performed to monitor the change of surface coverage and surface electronic properties during the native oxide growth of initially H-terminated Si(111) and Si(100) surfaces in water and air.

Wafers with a thin oxide layer were modelled by a layer of SiO_2 on top of c-Si using the data from the initially H-terminated sample before oxidation to include the varying fraction of roughness remaining after the H-termination procedure on Si(100) and Si(111) surfaces. Fig. 3 presents the evolution of oxide thickness $\langle d_{ox}\rangle$ on initially H-terminated Si(111) and Si(100) surfaces during the hot water treatment at 80°C. The Si(100) oxidizes faster than Si(111). However, the resulting native oxide thickness reaches 1.5–2 nm on Si(111) and 2.5–3 nm on Si(100) substrates.

In order to compare the stability of the surface passivation by hydrogen, identically prepared H-terminated Si(111) and Si(100) surfaces were repeatedly characterized by FT-IR SE measurements during storage in clean-room air. The Si–H and Si(–H)$_2$ bonds on H-terminated wafers were directly-detected by IR SE measurements. According to our measurements the bond vibrational stretching resonance on the completely H-terminated Si(111) surface immediately after preparation causes a maximum difference δ_{max} in the Δ spectrum of approximately 0.4° and a minimum in the tan Ψ spectrum obtained at the resonance position 2083 cm^{-1} (Fig. 4). On H-terminated Si(100) surfaces, a dispersion-like structure in Delta with $\delta_{max}\approx 0.1°$ at 2102 cm^{-1} is found, unambiguously caused by the Si(–H)$_2$ bond.

Fig. 5a shows the decrease of the relative number $N_{rel} = \delta/\delta_{max}$ of the Si(–H)$_2$ and Si–H oscillators which is directly proportional to the number of Si(–H)$_2$ on the Si(100) surface and Si–H bonds on the Si(111) surface, respectively [13].

The increasing effective thickness $\langle d_{ox}\rangle$ of the native oxide film as a function of storage time in air was derived from UV–VIS SE measurements on the same

samples (Fig. 5b). During the formation of a first oxide monolayer — the so-called initial phase of oxidation —, a continuous reduction in the number of Si–H as well as Si(–H)$_2$ bonds complementary to native oxide growth was observed. When the hydrogen completely disappeared, the effective thickness $\langle d_{ox} \rangle$ of the native oxide film increased and the surface state distribution change drastically. The native oxide grown in air resulted in a rather high surface density of $D_{it,\ min} > 10^{12}$ eV^{-1} cm^{-2}. While successfully H-terminated Si(111) surfaces are stable against re-oxidation in air for 24–48 h, the duration of the initial phase of oxidation was found to be significantly shorter on Si(100) surfaces.

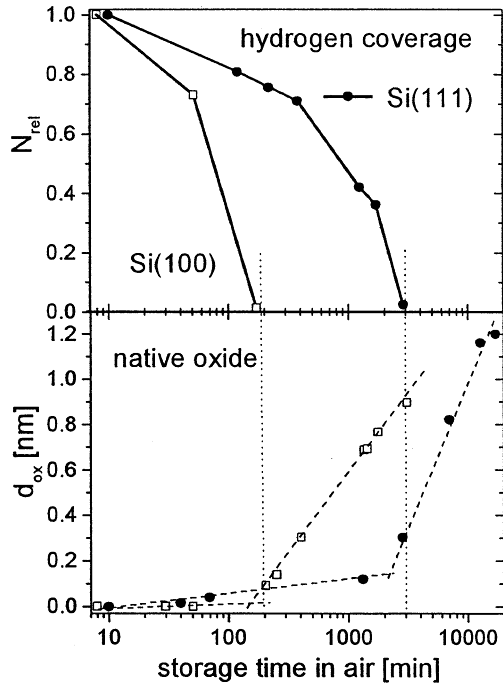

Fig. 5. The relative number of Si–H and Si(–H)$_2$ bonds respectively (a) and the effective oxide thickness (b) on a H-terminated Si(111) and Si(100) surface versus the storage time in air.

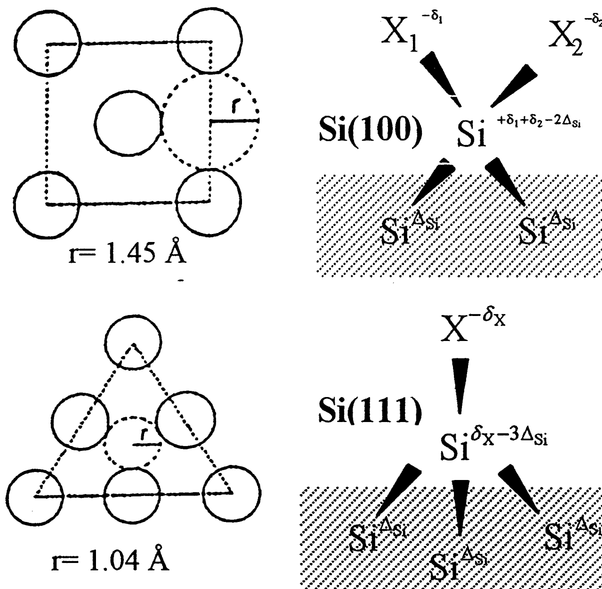

Fig. 6. Schematic diagram of the atom void radius r and back bond polarization (ΔSi and δY) for crystalline Si (100) and Si(111) surfaces.

5. Discussion

Summarizing the results, generally higher surface and interface state densities were observed on H-terminated and HF-treated as well as on natively oxidized Si(100) surfaces in comparison to Si(111). On successfully prepared H-terminated Si(111) and Si(100) surfaces, the density of states could be directly correlated to the surface roughness; very low surface state densities $D_{it,min}$ of about 10^{10} cm^{-2} eV^{-1} on the Si(111) surfaces with atomically flat areas and half of a magnitude higher values of $D_{it,min}$ about 5×10^{10} cm^{-2} eV^{-1} on atomically rough Si(100) were obtained. Due to their selective etching behavior, NH_4F and HF-solutions cause differences in surface morphology depending on the substrate orientation. Therefore, during HF-treatment the surface roughness on Si(111) increased more than on Si(100) substrates. Nevertheless, on HF-treated Si(111) surfaces also lower surface state densities were found. Fig. 6 describes the configuration of surface atoms on Si(111) and Si(100), substrates. While the wet-chemically treated Si(111) surface is characterized by one dangling bond or electronegative substituent per atom, on Si(100) surface atoms two dangling bonds or adatoms are possible.

We regard the higher density of surface states to be the reason for the lower stability of H-terminated Si(100) surfaces against reoxidation in air. Moreover, the electronegativity difference between the two substituents (-H, -OH, -F) and the Si surface atom results in a stronger polarization of the Si back bond on Si(100) substrates, which leads to a heavy attack of nucleophilic species (O_2, H_2O). Therefore, the initial phase of oxidation on Si(100) is significantly shorter than that on Si(111) substrates. However, compared to the Si(111) wafers, on Si(100) substrates a faster oxide growth and a thicker final oxide layer were found. These differences can be explained by the greater atom distance on Si(100) surfaces shown in Fig. 6. Independent of the kind of treatment, on wet-chemically oxidized Si(100) surfaces also higher interface state densities were observed, caused by the faster oxide growth.

6. Summary

As demonstrated in this article, the combination of SPV and SE measurements as non-destructive surface sensitive methods can be successfully applied for controlling and optimizing the wet-chemical treatment during the technological process. In contrast to ATR spectroscopy, FT-IR SE applies only a single reflection for sensing the Si–H vibrational resonance and can therefore be used for standard wafer characterization. Correlation between the surface roughness, the hydrogen and oxygen coverage, and the surface states were investigated on Si(100) surfaces and compared to recent findings obtained on Si(111) surfaces. Considering the differences between the surface properties and reactions discussed here, the preparation of hydrogen or oxide passivated surfaces on Si(100) substrates by wet-chemical preparation methods has been carefully optimized aimed at smooth H-terminated Si(100) surfaces with low surface state densities. By the hot water oxidation of these H-terminated Si(100) surfaces very thin passivation layers in the thickness range of 1–3 nm characterized by interface state densities $D_{it,min} < 5 \times 10^{11}$ eV^{-1} cm^{-2} were prepared.

Acknowledgements

The work was partially supported by the BMBF under contract No. 329773.

References

[1] T. Hattori, Surface Processing of Silicon Wafers, Springer, Heidelberg, 1998, pp. 437.
[2] Y.A. Chabal, G.S. Higashi, K. Raghavachari, V.A. Burrows, J. Vac. Sci. Technol. A7 (3) (1989) 2104.
[3] M. Grundner, H. Jacob, Appl. Phys. A39 (1986) 73.
[4] T. Konishi, T. Yao, M. Tajima, H. Ohshima, H. Ito, T. Hattori, Jpn. J. Appl. Phys. 31 (1992) L1216.
[5] N. Hirashita, M. Kinoshita, I. Aikawa, T. Ajioka, Appl. Phys. Lett. 56 (5) (1990) 451.
[6] M. Niwano, Y. Takeda, K. Kurita, N. Miyamoto, J. Appl. Phys. 72 (6) (1992) 2488.
[7] H. Angermann, A. Röseler, M. Rebien, W. Henrion, Proceedings of the 7th Intern. Symp. on Semiconductor Manufacturing (ISSM), Tokyo, Japan, 1998, p. 137.
[8] H. Angermann, W. Henrion, M. Rebien, K. Kliefoth, D. Fischer, J.T. Zettler, Microelectron. Eng. 36 (1997) 43.
[9] W. Kern, Surf. Sci. 31 (1970) 207.
[10] H. Angermann, K. Kliefoth, H. Flietner, Appl. Surf. Sci. 104/105 (1995) 107.
[11] K. Heilig, Solid State Electron. 27 (4) (1984) 395.
[12] G.S. Higashi, Y.J. Chabal, G.W. Trucks, K. Raghavachari, Appl. Phys. Lett. 56 (7) (1989) 656.
[13] A. Röseler, Infrared Spectroscopic Ellipsometry, Akademie-Verlag, Berlin, 1990, p. 15.
[14] A. Röseler, J. Opt. Soc. Am. A9 (7) (1992) 1124.
[15] H.J. Lewerenz, T. Bitzer, J. Electrochem. Soc. 139 (2) (1992) L21.
[16] D.E. Aspnes, Phys. Rev. B41 (15) (1990) 10334.
[17] D.A.G. Bruggeman, Ann. Phys. Leipzig 24 (1935) 636.
[18] T. Yasuda, D.E. Aspnes, Appl. Opt. 33 (31) (1994) 7435.
[19] H. Flietner, Mater. Sci. Forum 185 (188) (1995) 73.